Exploring fissure opening and their connectivity in a Cenozoic clay during gas injection

Laura Gonzalez-Blanco[1], Enrique Romero[1], Cristina Jommi[2], Xavier Sillen[3], Xiangling Li[4]

[1]Universitat Politècnica de Catalunya, Barcelona, Spain

[2]Delft University of Technology, Delft, The Netherlands

[3]ONDRAF/NIRAS, Brussels, Belgium

[4]EIG EURIDICE, Mol, Belgium

Gas transport properties in argillaceous rocks are becoming an important issue within different contexts of energy-related geomechanics (disposal of radioactive waste, production of shale gas, CO_2 sequestration). The present investigation aims at describing the pathways generated on a deep Cenozoic clay during gas injection using different microstructural techniques. Mercury intrusion porosimetry results have allowed detecting fissures after gas injection tests that have not been observed on intact samples. The opening of these pressure-dependent fissures plays a major role on gas permeability. A complementary insight into the connectivity of these fissures has been quantified by micro-computed tomography.

Introduction

The migration of gases through argillaceous rocks is an important issue in energy-related geoengineering applications, such as CO_2 geological sequestration, extraction of gas shale and nuclear waste geological storage. Within this last context, gases can be produced in the post-closure phase of the disposal system and may have a significant impact on the long-term performance of the host rock formation (ONDRAF/NIRAS, 2013; Shaw, 2013). The pressure resulting from the gas generation in an almost impermeable host rock will increase, and micro-cracks and fissures (gas pathways) may develop as a consequence of the deformation induced by stress and gas pressure changes, as well as by taking advantage of the material heterogeneity, anisotropy or rock discontinuities. These pathways have an important impact on gas intrinsic permeability, as a consequence of the strongly coupled response of the gas flow and the mechanical behaviour.

Evidence of fissure opening induced by air injection has been detected with mercury intrusion porosimetry (MIP) (Gonzalez-Blanco *et al.*, 2016). This technique

presents data on entrance pore sizes and their distribution, but does not provide information on their shape (pore or fissure) – unless fractal analysis is used – or on their connectivity. The use of new tomographic techniques in the geotechnical field, such as X-ray micro-computed tomography (μCT), nuclear magnetic resonance (NMR) or focussed ion beam-scanning electron microscopy (FIB-SEM), appear to be encouraging to complement the microstructural characterisation (Muurinen *et al*., 2013; Fleury & Canet, 2014; Desbois *et al*., 2014; Hemes *et al*., 2015).

This work particularly addresses the changes in the pore network of Boom Clay induced by air injection using MIP and μCT. Boom Clay is a potential Cenozoic sedimentary clay formation in Belgium for the geological disposal of long-living and heat-emitting radioactive waste. MIP tests will allow quantifying the pore volumes associated with the micro and macroporosity, as well as the pore size distribution changes before and after air injection, whereas μCT images will be mainly used to quantify the connectivity of the pore network.

Air injection tests on Boom Clay

Boom Clay (Northwest European Tertiary Basin) with dominant kaolinitic-illitic clay fraction was retrieved at a depth of 223 m in the Underground Research Laboratory facility of EURIDICE at Mol, Belgium. The void ratio of the retrieved clay was between 0.56 and 0.61 with an air-entry value around 4.8 MPa. Main geotechnical properties are described in Gonzalez-Blanco *et al*. (2016).

An instrumented high-pressure and high-stiffness oedometer cell (20-mm thick samples and 50 mm in diameter) was used to perform the air tests and to determine the soil volume changes during air injection and dissipation stages. The air injection (bottom cap) was performed at a constant volume-rate of 100 mL/min on a sample with bedding planes parallel to air flow and at a constant total vertical stress of 6 MPa (A to B in Fig. 1). When air pressure reached a maximum of 4 MPa (below the air-entry value of the material), the air injection piston was stopped (shut-off at point B in Fig. 1), and then allowed decaying at constant air volume of the inlet line (B to C in Fig. 1). The sample at constant total vertical stress displayed some small expansion (negative volumetric strain) during the air injection stage. After shut-off, expansion continued as the air pressure front propagated into the sample, inducing the pore fluid pressure to increase and the constitutive stress to decrease. Some elapsed time later after shut-off, the air injection pressure started to decline along the dissipation stage towards point C with a sharp increase of the outflow volume through the top cap (upper graph in Fig. 1). Consequently, the constitutive stress increased inducing compression on the material. The expansion deformation induced during the air injection and early shut-off stages may cause some damage on the material (Gonzalez-Blanco *et al*., 2016).

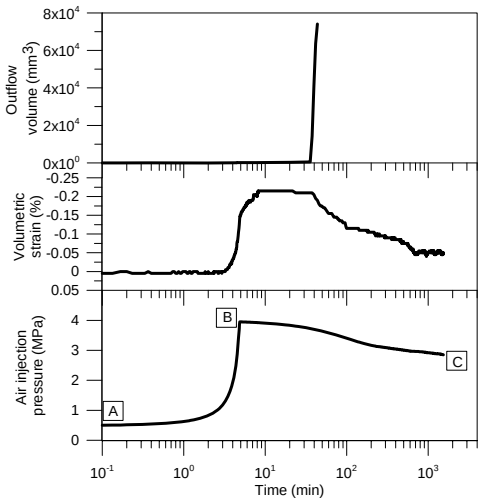

Fig. 1. Time evolution of outflow volume, volumetric strain and air injection pressure during the air injection / dissipation test (A to B: air injection stage; B: shut-off; B to C: dissipation stage).

Mercury intrusion porosimetry

MIP tests were performed on intact Boom Clay and after air injection tests (Autopore IV 9500, Micrometrics). Instantaneous freezing was carried out by plunging small samples (around 1000 mm^3) into liquid nitrogen and then applying vacuum to ensure microstructure preservation. Desbois *et al*. (2014) showed that no significant changes in the quantification of pore sizes and pore morphologies were produced due to this sublimation process.

Fig. 2a presents the pore size density functions for the intact material and after the air tests in terms of the intruded volume of mercury referred to the volume of solids (non-wetting void ratio e_{nw}) for different entrance pore sizes x (Romero & Simms, 2008). As indicated in the figure, a new family of large pores, which was not detected on intact samples and on loaded samples without air injection, was observed after the air tests. This new dominant pore size at entrance sizes larger than 2 μm appeared to be associated with the expansion undergone by the material during the air injection and early shut-off stages and the possible opening of fissures (Gonzalez-Blanco *et al*., 2016). MIP data were also interpreted in terms of the fractal character of the porous network admitting self-similarity of the hierarchical void structure. Fig. 2b shows the fractal dimensions D_s of the porous medium on intact material and after the air tests, obtained from the change of the intruded degree of saturation Sr_{nw} with respect to the change in injection pressure p. As observed, the fractal analyses suggested a fissure-like structure after the air tests.

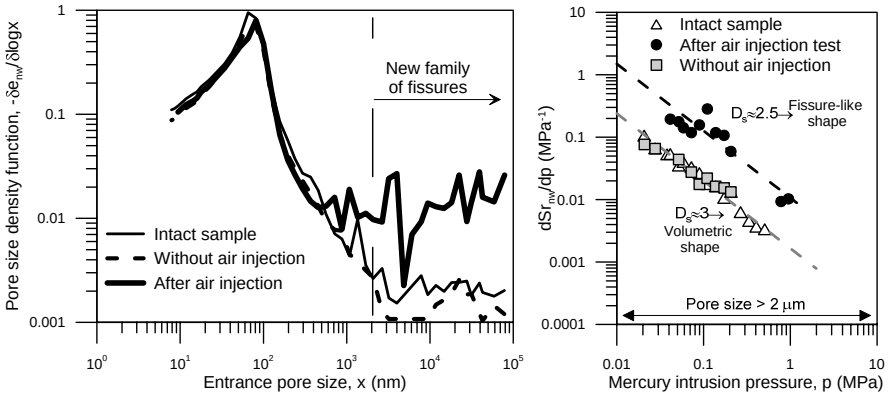

Fig. 2. a) Pore size density function changes before and after air tests. b) Fractal analyses of MIP results showing fissure-like shape after the air tests.

Micro-computed tomography and image analyses

μCT scans were carried out on a Phoenix Nanotom equipment (GE Oil & Gas) to analyse the internal 3D microstructure of the intact material and after the air tests (Andò *et al*., 2011; Josh *et al*., 2012; Saba *et al*., 2014; Deng *et al*., 2016). Although the technique did not need any sample pre-treatment, the same freeze-drying process as in the MIP tests was followed for further comparison of results. The samples (15 mm height, 15 mm in diameter) were scanned using 720 projections on 360º with a voxel size of 20 μm. The final 3D images were 16-bit grayscale with a size of 825 × 825 × 875 voxels.

Fig. 3 presents two slices that corresponded to intact material and after the air test. Differences between them could be readily observed: the intact sample presented a homogeneous aspect (except for calcium carbonate inclusions in white due to their higher density), whereas after the air injection test some fissures were visible throughout the cross-section that were oriented along bedding planes.

The main goal of the image analysis was to study fissures induced by the air passage, as well as to quantify their total volume and connectivity. The multiscale Hessian fracture filtering (Voorn *et al*., 2013) was used to analyse μCT-scan images. It was implemented in a multiplatform of the public domain software ImageJ (Rasband, 2012) that allowed the segmentation of narrow fractures in 3D image data. The connectivity filtering, which works through a MATLAB® script, allowed generating the connected fracture pattern.

After multiscale filtering, the fissures obtained using adequate parameters are depicted in Fig. 4, where two types of fissures can be distinguished: the connected

ones in green and the non-connected in maroon. The figure also shows the total volume of the sample, in which the bedding plane orientation is indicated with a blue plane. The fissure pattern was consistent with the opening of fissures during the expansion undergone by the material along the air injection and early shut-off stages and revealed that the air pathways followed the bedding planes.

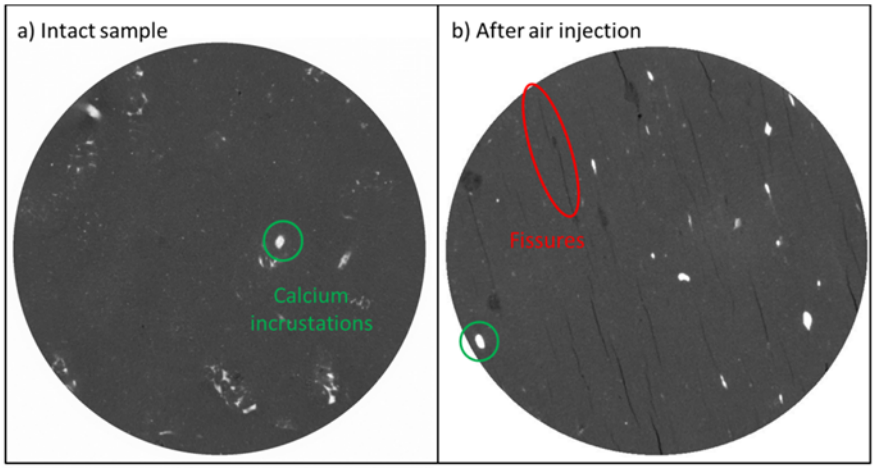

Fig. 3. µCT images of intact sample (left) and after the air tests (right).

Quantitative comparison of both techniques

This section compares the volume of fissures induced by the air tests obtained by both techniques. As previously indicated, MIP results considered fissures with entrance sizes larger than 2 µm, whereas µCT voxel resolution was limited to 20 µm. Therefore, only fissures larger than 20 µm were considered to obtain comparable results between both techniques.

A fissured void ratio $e_{fissured}$, defined as the area below the pore size density function after the air test (Fig. 2a), was used to quantify the volume of fissures (respect to the volume of solids) induced by air migration (refer to Table 1). This fissured void ratio was normalised with respect to the total void ratio e = 0.56 ($e_{fissured}/e$ in Table 1).This ratio was useful to provide information on the expected value of the final degree of saturation of the clay after the air tests, $Sr = 1\text{-}e_{fissured}/e$, when all fissures were desaturated (and clay matrix pores were still saturated). Final Sr = 0.932 and 0.953 could be estimated when all fissures larger than 2 µm and 20 µm, respectively, were desaturated.

The quantitative analysis of the fissures (x > 20 µm) obtained after the filtering process of the µCT images resulted in a fissured volume of 34.5 mm^3, of which only

8.6 mm^3 were connected. The total volume of the analysed sample was 1900 mm^3 (volume of solids: 1218 mm^3). The fissured void ratio obtained by this technique is also reported in Table 1. As observed, only 25% of the fissures were connected, which indicated a final degree of saturation after the tests of Sr = 0.987 if only connected fissures larger than 20 μm were desaturated.

A good consistency is observed in the table for $e_{fissured}$ when comparing both techniques at the same range of fissure sizes (x > 20 μm).

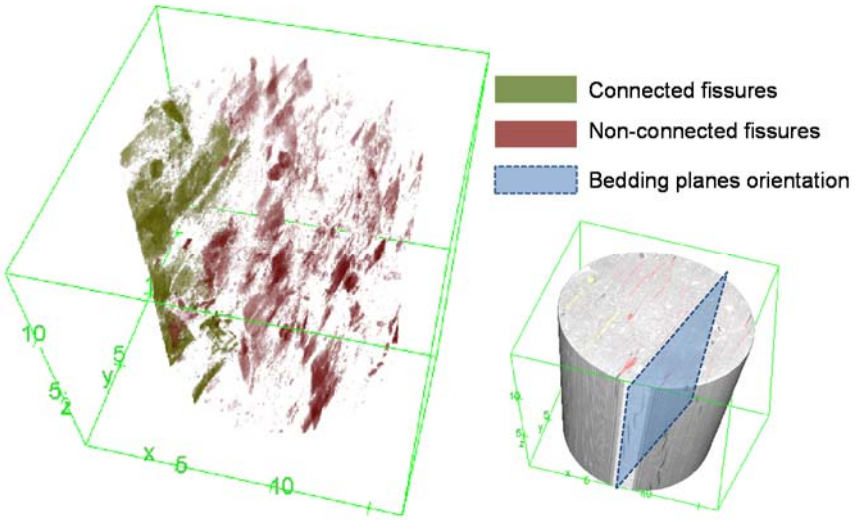

Fig. 4. 3D reconstruction of the fissure pattern in the sample after the multiscale Hessian and connectivity filtering (left) together with the total volume of the sample (right).

Table 1. Quantification of fissured void ratios using MIP and μCT results.

Technique	$e_{fissured}$	$e_{fissured}/e$
MIP (x > 2 μm)	0.038	0.068
MIP (x > 20 μm)	0.026	0.047
μCT (x > 20 μm, all fissures)	0.028	0.050
μCT (x > 20 μm, connected fissures)	0.007	0.013

Concluding remarks

Air injection / dissipation stages on Boom Clay systematically displayed expansion deformation that induced damage on the material and the opening of preferential air pathways (fissures). These fissures played a major role on the dissipation stage, in which the air injection pressure started to decline with a sharp increase of the outflow air volume.

Two different microstructural techniques were used to analyse the changes in the pore network before (on intact material) and after the air test, namely mercury intrusion porosimetry (MIP) and micro-computed tomography (μCT).

MIP provided information on the entrance pore sizes and the distribution of the pore space (pore size density function), which resulted in the detection of a new family of pores at entrance sizes larger than 2 μm after the air passage. The technique also allowed the quantification of the volume of fissures larger than 2 μm. A fractal analysis of the mercury intrusion data confirmed this fissure-like structure after the air test.

μCT images also confirmed the existence of fissures after the air test that followed the orientation of the bedding planes. Image analysis through multiscale Hessian fracture filtering allowed the quantification of the volume of fissures after the air tests. To obtain comparable results between both techniques, only fissures larger than 20 μm (μCT voxel resolution) were considered. The volume of fissures respect to the volume of solids (fissured void ratio) was 0.026 and 0.028 for MIP and μCT, respectively. In addition, the image analysis allowed quantifying the connectivity of the fissure network, resulting in 25% of connected fissures. This information was useful to provide the expected value of the final degree of saturation of the clay after the air test, when all connected fissures larger than 20 μm were desaturated (Sr = 0.987).

Acknowledgements

The authors are grateful to the Belgian agency for radioactive waste management (ONDRAF/NIRAS) for their financial support (‘Laboratory investigation of the gas transport processes in a repository located in Boom Clay’, ref. XSI/AV/2012-1952, 2012-2016).

References

Andò E, Hall S.A, Viggiani G (2011) Grain-scale experimental investigation of localised deformation in sand: a discrete particle tracking approach. Acta Geotech. 7(1): 1-13. doi: 10.1007/s11440-011-0151-6.

Desbois G, Urai J.L, Hemes S, Brassinnes S, De Craen M, Sillen X (2014) Nanometer-scale pore fluid distribution and drying damage in preserved clay cores from Belgian clay formations inferred by BIB-cryo-SEM. Engineering Geology 179(4): 117-131. doi: 10.1016/j.enggeo.2014.07.004.

Deng H, Fitts J.P, Peters C.A (2016) Quantifying fracture geometry with X-ray tomography: Technique of Iterative Local Thersholding (TILT) for 3D image segmentation. Comput. Geosci. 20(1): 231-244. doi: 10.1007/s10596-016-9560-9.

Fleury M., Canet D. (2014) Water orientation in smectites using NMR nutation experiments. J. Phys. Chem. C., 118(9): 4733-4740. doi: 10.1021/jp4118503.

Gonzalez-Blanco L, Romero E, Jommi C, Li X, Sillen X (2016) Gas migration in a Cenozoic clay: experimental results and numerical modelling. Geomechanics for Energy and the Environment 6: 81-100. doi: 10.1016/j.gete.2016.04.002.

Hemes S., Desbois G., Urai J.L., Schöppel B., Schwarz J-O. (2015) Multi-scale characterization of porosity in Boom Clay (HADES-level, Mol, Belgium) using a combination of X-ray μ-CT, 2D BIB-SEM and FIB-SEM tomography. Microporous and Mesoporous Materials 208: 1-20. doi: 10.1016/j.micromeso.2015.01.022.

Josh M, Esteban L, Delle Piane C, Sarout J, Dewhurst D.N, Clennell M.B (2012) Laboratory characterization of shale properties. J. Petroleum Science Engineering 88-89: 107-124. doi: 10.1016/j.petrol.2012.01.023.

Muurinen A., Carlsson T., Root A. (2013) Bentonite pore distribution based on SAXS, chloride exclusion and NMR studies. Clay Minerals 48(2): 251-266. doi: 10.1180/claymin.2013.048.2.07

ONDRAF/NIRAS (2013) Research, Development and Demonstration (RD&D) Plan for the geological disposal of high-level and/or long-lived radioactive waste including irradiated fuel of considered as waste, State-of-the-art report as of December 2012," ONDRAF/NIRAS, Rep NIROND-TR 2013-12 E, 2013.

Rasband W.S (2012) Image J. U.S. National Institutes of Health, Bethesda, Maryland, USA. http://imagej.nih.gov/ij/

Romero E, Simms P.H (2008) Microstructure investigation in unsaturated soils: A review with special attention to contribution of mercury intrusion porosimetry and environmental scanning electron microscopy. Geotechnical and Geological Engineering 26(6): 705-727. doi: 10.1007/s10706-008-9204-5.

Saba S, Delage P, Lenoir N, Cui Y.J, Tang A.M, Barnichon J.D (2014) Further insight into the microstructure of compacted bentonite-sand mixture. Engineering Geology 168: 141-148. doi: 10.1016/j.enggeo.2013.11.007.

Shaw R.P. (Ed). (2013) Gas Generation and Migration. In International Symposium and Workshop 5th to 7th February 2013 Luxembourg, Proceedings FORGE Report, 269 p.

Voorn M, Exner U, Rath A (2013) Multiscale Hessian fracture filtering for the enhancement and segmentation of narrow fractures in 3D image data. Comput. Geosci. 57: 44-53. doi: 10.1016/j.cageo.2013.006.